

1 **The impact of organic nitrates on summer ozone formation in Shanghai,**
2 **China**

3 Chunmeng Li¹, Xiaorui Chen^{2, 3*}, Haichao Wang^{2, 3}, Tianyu Zhai⁴, Xuefei Ma⁵, Xinping Yang⁴, Shiyi
4 Chen⁵, Min Zhou⁶, Shengrong Lou⁶, Xin Li⁵, Limin Zeng⁵, Keding Lu^{5*}

5 ¹ Center for Environmental Metrology, The National Institute of Metrology, Beijing 100029, China.

6 ² School of Atmospheric Sciences, Sun Yat-sen University, Zhuhai, Guangdong, 519082, China.

7 ³ Guangdong Provincial Observation and Research Station for Climate Environment and Air Quality
8 Change in the Pearl River Estuary, Key Laboratory of Tropical Atmosphere-Ocean System, Ministry
9 of Education, Southern Marine Science and Engineering Guangdong Laboratory (Zhuhai), Zhuhai,
10 519082, China.

11 ⁴ State Environmental Protection Key Laboratory of Vehicle Emission Control and Simulation,
12 Chinese Research Academy of Environmental Sciences, Beijing, 100012, China

13 ⁵ State Key Joint Laboratory of Environmental Simulation and Pollution Control, The State
14 Environmental Protection Key Laboratory of Atmospheric Ozone Pollution Control, College of
15 Environmental Sciences and Engineering, Peking University, Beijing, 100871, China.

16 ⁶ State Environmental Protection Key Laboratory of the Cause and Prevention of Urban Air Pollution
17 Complex, Shanghai Academy of Environmental Sciences, Shanghai, 200233, China.

18
19 * Correspondence: chenxr95@mail.sysu.edu.cn; k.lu@pku.edu.cn

20 **Abstract**

21 Organic nitrates serve as important secondary oxidation products in the atmosphere, playing a crucial
22 role in the atmospheric radical cycles and influencing the production of secondary pollutants (ozone
23 (O₃) and secondary organic aerosols). However, field measurements of organic nitrates are scarce in
24 China, and a comprehensive localized mechanism for organic nitrates is absent, hindering effective
25 pollution mitigation strategies. In this study, we conducted measurements of ambient gaseous organic
26 nitrates and examined their effects on local O₃ production at a polluted urban site in eastern China
27 during summer. The average daytime concentrations of alkyl nitrates (ANs) and peroxy nitrates (PNs)
28 throughout the campaign were 0.5±0.3 ppbv and 0.9±0.7 ppbv, respectively, with peaks reaching up to
29 1.6 ppbv and 3.6 ppbv. An observation-constrained box model, incorporating an updated mechanism
30 for organic nitrates, was employed to assess the environmental impact of these compounds. The model
31 results indicated that PNs production inhibited the daytime O₃ production by 16% (0.8 ppbv/h), which
32 is relatively low compared to previous studies. Furthermore, scenario analyses revealed that production
33 yields (α) of ANs would alter the response of O₃ formation to precursors due to varying compositions
34 of volatile organic compounds. Our results suggest that blind pollution control may cause ineffective
35 pollution prevention and highlight the necessity of a thorough understanding on organic nitrate

36 chemistry for local O₃ control strategy.

37 **1. Introduction**

38 Tropospheric ozone, as an important oxidant, influences the atmospheric lifetimes of trace gases
39 through its involvement in photochemical processes, thereby playing a crucial role in climate change
40 and atmospheric chemistry. There is a broad consensus that high near-surface ozone concentrations are
41 hazardous to human health and environmental ecosystems, particularly affecting the human respiratory
42 and cardiovascular systems, and result in decreased yields of various crops (Ashmore, 2005; Xue and
43 Zhang, 2023). A scientific assessment of tropospheric ozone is essential for the development of public
44 health policies and for addressing long-term air pollution challenges (Monks et al., 2015). Primary
45 pollutants, such as nitrogen oxides (NO_x) and volatile organic compounds (VOCs), participate in the
46 formation of HO_x radicals (RO_x = RO₂ + HO₂ + OH) cycles and NO_x cycles under sunlight, leading to
47 the continuous production of ozone as a secondary oxidation product within these cycles. In addition
48 to the reaction between OH and NO₂ that produces HNO₃ as part of chain termination reactions, the
49 interaction of RO₂ and NO that produces organic nitrates is of increasing concern (Present et al., 2020).
50 The atmospheric production of organic nitrates consumes both NO_x and RO₂. Therefore, the chemistry
51 of organic nitrates will significantly influence the prevention and control of ozone, with NO_x and VOCs
52 serving as independent variables.

53 Both anthropogenic activities and natural processes contribute to the emissions of NO_x and VOCs,
54 which produce RO₂ in the presence of oxidants such as OH. Subsequently, RO₂ reacts with NO to yield
55 NO₂ and RO. After that, NO₂ photolysis produces O₃, while RO is converted into HO₂ through an
56 isomerization reaction, thereby forming the ozone production cycle. Within the cycle, a branching
57 reaction between RO₂ and NO leads to the formation of alkyl nitrates (RONO₂, ANs), while RO₂ may
58 also react with NO₂ to generate peroxy nitrates (RO₂NO₂, PNs). Given that PNs are prone to thermal
59 dissociation near the surface (Roberts and Bertman, 1992), they can influence O₃ production by
60 modifying the availability of NO_x and RO_x. Due to the competitive production dynamics between PNs
61 and O₃, numerous field observations and model simulations have been conducted to investigate the
62 impact of peroxyacetyl nitrate (PAN) on O₃ production (Liu et al., 2021; Zeng et al., 2019; Zhang et
63 al., 2020). For ANs formation, the branching ratio (α), the reaction ratio $k_{1b}/(k_{1a}+k_{1b})$, varies between
64 0.1-35%, which are associated with the carbon chain structure of the molecule, the distribution of
65 functional groups, temperature, and pressure (Reisen et al., 2005; Arey et al., 2001; Wennberg et al.,
66 2018; Russell and Allen, 2005; Butkovskaya et al., 2012; Cassanelli et al., 2007). Some values of α ,
67 which have not been quantified in the laboratory, are estimated through structure-activity relationships
68 (Arey et al., 2001; Reisen et al., 2005; Teng et al., 2015; Yeh and Ziemann, 2014a; Yeh and Ziemann,
69 2014b). Multiple field observations revealed a strong linear correlation between ANs and O₃, with a
70 correlation coefficient (r^2) exceeding 0.5, further substantiating the competitive relationship between
71 ANs and O₃ (Aruffo et al., 2014; Day et al., 2003; Flocke et al., 1998).



74 Currently, research on the effects of ANs on O₃ distribution is predominantly located in Europe
75 and the United States. Following the first in situ measurement of total organic nitrates through thermal
76 dissociation laser-induced fluorescence instrument (TD-LIF) by Day et al., field observations of total
77 ANs have been continuously conducted to study the role of ANs in the nitrogen cycle (Aruffo et al.,

78 2014; Browne et al., 2013; Chen et al., 2017; Darer et al., 2011; Day et al., 2003; Sadanaga et al., 2016).
79 In conjunction with field observations and model simulations, Farmer et al. were the first to indicate
80 that ANs influence the sensitivity of NO_x-VOCs-O₃ (Farmer et al., 2011). As NO_x emissions decrease
81 due to pollution control measures, ANs chemistry is expected to play an increasingly significant role
82 in O₃ simulations (Present et al., 2020; Zare et al., 2018). Current mechanisms for O₃ simulations
83 generally achieve reasonable predictions in large-scale models; however, they exhibit deviations
84 exceeding 10 ppbv in regional simulations (Young et al., 2018). Subsequent studies have demonstrated
85 that refining the ANs chemistry can further improve the simulation performance for O₃ (Schwantes et
86 al., 2020). ANs are predominantly produced through oxidation reactions facilitated by OH, O₃, and
87 NO₃. The daytime ANs are mainly contributed by the OH channel, whereas during nighttime, the
88 contribution of the NO₃ channel is linked to significantly increased yields of ANs (Liebmann et al.,
89 2018; Ng et al., 2017; Zare et al., 2018). Presently, the enhancement of ANs chemistry mainly focuses
90 on BVOCs, particularly isoprene and monoterpenes. These researches aim to enhance the yield of ANs
91 derived from BVOCs, the re-release ratio of ANs to NO_x, and the contribution of ANs to aerosols
92 (Fisher et al., 2016; Romer et al., 2016; Travis et al., 2016; Zare et al., 2018). Despite the establishment
93 of a complete mechanism scheme at present, significant uncertainties remain in ANs simulation, which
94 may introduce substantial uncertainties into the O₃ simulation.

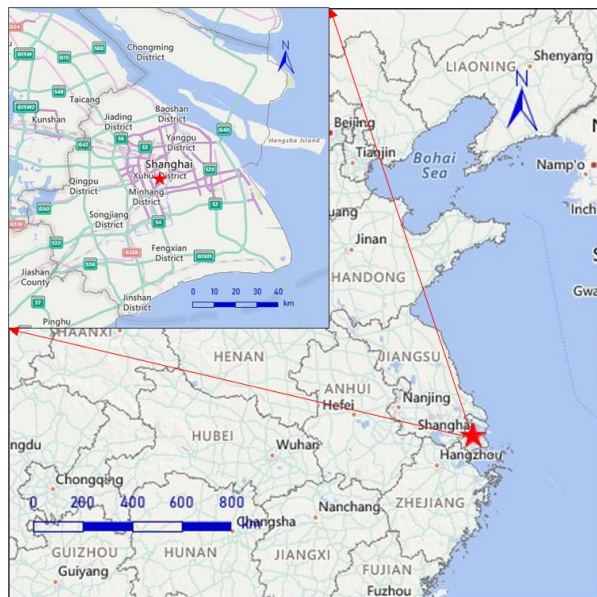
95 Atmospheric pollution is common across China, particularly in the Yangtze River Delta. Shanghai,
96 as a highly urbanized metropolis in the Yangtze River Delta, has rendered the region's complex
97 pollution due to its rapid economic growth and urbanization (Wang et al., 2022; Zhu et al., 2021).
98 Previous studies have shown a significant increase in near-surface O₃ levels from 2006 to 2016 in
99 Shanghai (Gao et al., 2017). However, research on the ANs chemistry and their impact on O₃ pollution
100 remains limited in this area. In addition, most field measurements of ANs have focused on short-chain
101 species (Ling et al., 2016; Song et al., 2018; Sun et al., 2018; Wang et al., 2013), which have been
102 observed to exert a typical inhibition effect on daytime O₃ production. A limited number of total ANs
103 measurements found that both ANs and O₃ production were in the VOC-limited regime (Li et al., 2023).
104 To further investigate the influence of organic nitrates on O₃ production, this study describes the
105 distribution of organic nitrates based on a comprehensive field campaign conducted in Shanghai,
106 analyzes the effects of organic nitrates on O₃ production through model simulations, and offers
107 recommendations for the prevention and control of ozone pollution in the region.

108 2. Methodology

109 2.1 Measurement site and instrumentations

110 A comprehensive campaign was conducted in Shanghai to further investigate the chemical
111 behavior of organic nitrates in urban environments across China. As depicted in Fig. 1, the site is
112 located in the Xuhui District of Shanghai (121.44°E, 31.18°N), in proximity to the Shanghai Inner
113 Ring Viaduct, surrounded by numerous residential and office areas without significant industrial
114 emission sources. The site is mainly influenced by morning-evening rush hours, as well as the transport
115 of air masses to the urban location. The overall wind speed was low, predominantly originating from
116 the east. All the measurement instruments were housed in the temperature-controlled room within the
117 laboratory building at the Shanghai Academy of Environmental Sciences. Thermal Dissociation-

118 Cavity Enhanced Absorption Spectroscopy (TD-CEAS) was positioned on the 7th floor about 25 m
119 above ground level, with the sampling tube extending out through the window.



120

121 **Figure 1.** Map of the city of Shanghai and the surrounding area (@ MeteoInfoMap). The red star is the location of
122 the campaign site.

123 The Shanghai campaign focused on studying summer ozone pollution, with the chemical
124 parameters presented in Table 1. Organic nitrates were measured by TD-CEAS with a sampling flow
125 rate of 3 L/min and a sampling duration of 3 min for alternating measurements of NO₂, PNs, and ANs.
126 The sampling apparatus consisted of a 2-meter-long 1/4-inch tetrafluoroethylene (TFE) tube, through
127 which the atmosphere was filtered through a TFE particulate filter. The membrane was replaced once
128 a day to mitigate the interference caused by wall loss. The measurement of PAN was conducted by gas
129 chromatography electron capture detection (GC-ECD). The Measurement of N₂O₅ was performed via
130 CEAS, which relies on the thermal dissociation of N₂O₅ to yield NO₃. Particulate nitrates and gaseous
131 HNO₃ were measured online by AeRosols and GAses (MARGA), where soluble substances were
132 quantified through ion chromatography following dissolution. The measurements of HONO were
133 finished by CEAS during the campaign. Measurements of VOCs were achieved using a combination
134 of GC-FID and GC-MS, with GC-MS predominating due to the limited species measured by GC-FID.
135 The photolysis rate constant (J value) was determined using a spectrum radiometer with a time
136 resolution of 20 s. Additionally, simultaneous measurements of other trace gases such as NO, NO₂,
137 SO₂, CO, O₃, and PM_{2.5} were conducted using commercial instruments.

138 **Table 1.** Measured species for organic nitrates analysis and instrument time resolution, accuracy, and detection
139 limitation.

| Parameters | Measurement technique | Time resolution | Accuracy | Detection limit |
|-------------------------------|-----------------------|-----------------|----------|-----------------|
| ANs, PNs, NO ₂ | TD-CEAS | 3 min | ± 8% | 93 pptv |
| PAN | GC-ECD | 5 min | ± 10% | 5 pptv |
| N ₂ O ₅ | CEAS | 1 min | ± 19% | 2.7 pptv |
| NO | Thermo 42i | 1 min | ± 10% | 60 pptv |

| | | | | |
|---------------------|-----------------------|-------|-------|-----------------------------------|
| NO ₂ | Chemiluminescence | 1 min | ± 10% | 300 pptv |
| HONO | CEAS | 1 min | ± 3% | 100 pptv |
| Particulate nitrate | 2060 MARGA | 1 h | ± 3% | 0.01 $\mu\text{g}/\text{m}^3$ |
| HNO ₃ | 2060 MARGA | 1 h | ± 3% | 0.01 $\mu\text{g}/\text{m}^3$ |
| SO ₂ | Thermo 43i-TLE | 1 min | ± 16% | 50 pptv |
| HCHO | Hantzschi fluorimetry | 1 min | ± 5% | 25 pptv |
| CO | Thermo 48i-TLE | 1 min | ± 16% | 50 pptv |
| O ₃ | Thermo 49i | 1 min | ± 5% | 0.5 ppbv |
| PM _{2.5} | Thermo TEOM | 1 min | ± 5% | 0.1 $\mu\text{g}/\text{m}^3$ |
| VOCs | GC-FID/GC-MS | 1 h | ± 30% | 20-300 pptv |
| J value | Spectrum radiometer | 20 s | ± 10% | $5 \times 10^{-5} \text{ s}^{-1}$ |

140

141 **2.2 Model calculation**

142 To investigate the impact of ANs chemistry on O₃ production, a box model was employed to
 143 simulate the photochemistry processes. The mechanism of the model was enhanced based on RACM2
 144 (Regional Atmospheric Chemical Mechanism version 2). This box model simulates the
 145 physicochemical processes occurring within a defined volume for each reactant. It utilizes measured
 146 parameters as the boundary condition to simulate the chemistry process while allowing for convenient
 147 adjustments to the mechanism. The model generates files detailing concentration changes, budget
 148 processes, and reaction rates, thereby providing an efficient means to simulate ground-level pollutants.
 149 In this study, the box model was constrained by various parameters, including J values, O₃, NO, NO₂,
 150 CO, HONO, VOCs, RH, temperature, and pressure, with the time step set to 1h. The deposition process
 151 was quantified using the deposition rate and the boundary layer height, with the dry deposition rate
 152 established at 1.2 cm/s and the boundary layer height constrained by data obtained from NASA.

153 The RACM2 facilitates classification through the distribution of functional groups and
 154 subsequently delineates reactions involving 17 stable non-organic compounds, 4 inorganic
 155 intermediates, 55 stable organic compounds, and 43 intermediate organic species within the
 156 mechanism. However, the mechanism description for ANs is notably abbreviated. The various ANs,
 157 characterized by differing functional groups, are treated as a unified entity, thereby neglecting the
 158 influence of functional groups on the underlying chemistry. Consequently, this study builds on the
 159 previous research and further evaluates the updates of the mechanism (Li et al., 2023). These
 160 mechanistic updates are developed based on the work of Zare et al. and primarily encompasses the
 161 oxidation processes of BVOCs by OH and NO₃, as well as the deposition and the aerosol uptake, which
 162 are detailed in the SI (Zare et al., 2018). Accordingly, three mechanistic schemas are compared based
 163 on the campaign, which will be elaborated upon in subsequent sections. A box model based on the
 164 above mechanism is used to calculate the ozone production rate (P(O₃)) (Tan et al., 2017b). P(O₃) was
 165 quantified based on the net production rate of O_x (the sum of O₃ and NO₂), by subtracting the O_x
 166 depletion from the instantaneous O_x production. The simulation uncertainty of the box model is about
 167 40%, introduced mainly by the simplified reaction rate constants, photolysis rate constants, and near-
 168 ground deposition (Lu et al., 2013). The impact of PNs photochemistry on local ozone is quantified by
 169 comparing the difference of the daytime P(O₃) between the scenarios with and without PNs

170 photochemistry via a chemical box model. Here, the PNs photochemistry includes the production and
171 removal of PAN, MPAN and PPN.

172 To facilitate the assessment of the impacts of ANs on local O₃ pollution, we further conducted a
173 simplified box model based on the steady-state assumption approach. Several studies have examined
174 the combined effect of α and VOCs reactivity on local O₃ levels using this approach (Farmer et al.,
175 2011; Present et al., 2020; Romer et al., 2016; Romer et al., 2018). Briefly, the production pathway of
176 ANs is simplified according to VOCs categories and the production rate of OH and HO₂ (P(HO_x)) is
177 fixed to a constant value. VOCs are categorized into two primary groups: non-oxygenated VOCs
178 (RVOCs) and oxygenated VOCs (OVOCs). Both categories of VOCs undergo oxidation by OH,
179 resulting in the formation of RO₂, specifically RVOCRO₂ and OVOCRO₂. The interaction between
180 RVOCRO₂ and NO will produce α ANs, (1- α) NO₂, HO₂, and OVOC. Conversely, the reaction of
181 OVOCRO₂ with NO directly generates NO₂. In the Beijing-Tianjin-Hebei, Yangtze River Delta, and
182 Chengdu-Chongqing regions of China, P(HO_x) is approximately 4 ppbv/h (Lu et al., 2013; Tan et al.,
183 2018a; Tan et al., 2018b). P(HO_x) is therefore assumed to be 4 ppbv/h, with equal production rates of
184 OH and HO₂. The model also incorporates additional processes, including inter- and self-reactions of
185 RO₂, as well as reactions between NO₂ and NO, and deposition processes. In addition, during the
186 daytime, NO is determined by $j(\text{NO}_2)$, O₃, and NO₂ according to the photo-stationary state among NO-
187 NO₂-O₃. Based on the above simplified approach, production rates of ANs and O₃ in this study can be
188 derived by direct calculations.

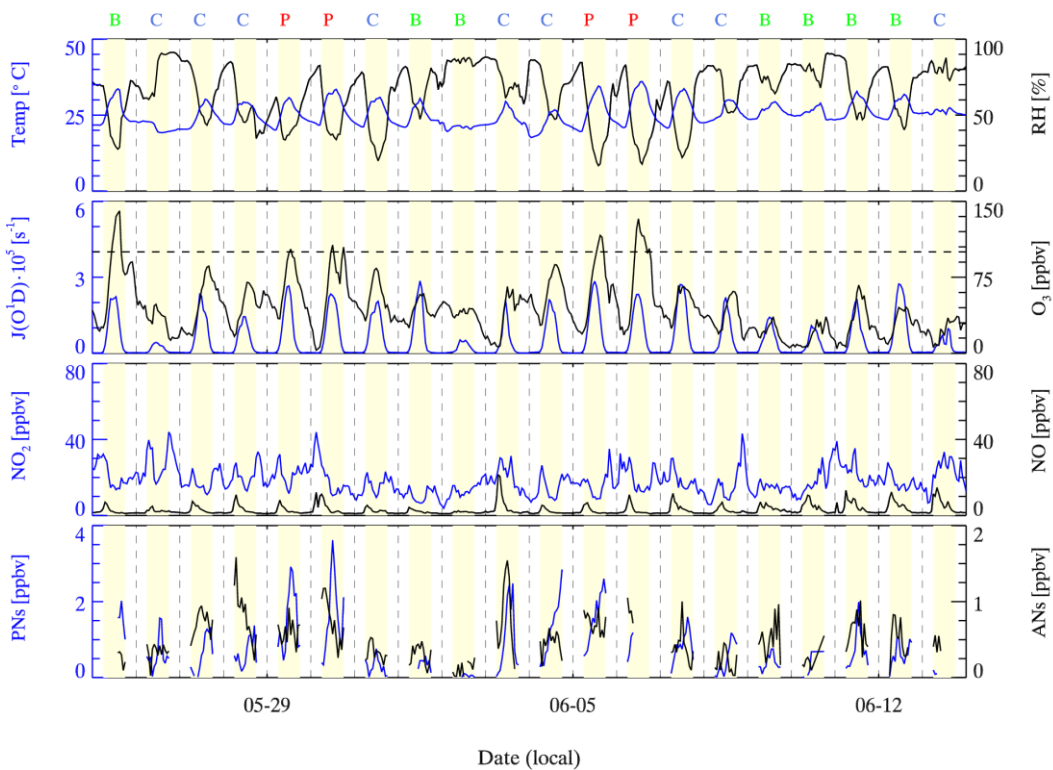
189 To investigate the effects of NO_x and VOCs on O₃ production, the theoretical maximum of P(O₃)
190 was simulated by a box model under varying concentrations of NO_x and VOCs. This approach was
191 employed to develop an empirical kinetic modeling approach for ozone production (EKMA). The
192 EKMA serves as a model sensitivity method to inform strategies for pollutant abatement. In this study,
193 EKMA utilizes the measured mean parameters as the initial point. Each parameter was incrementally
194 adjusted in 30 equidistant steps to create scaled arrays of VOCs and NO_x, which were subsequently
195 used to simulate the variations in P(O₃) resulting from changes in precursor concentrations. Ultimately,
196 contour plots illustrating the relationship between P(O₃) arrays versus the concentrations of NO_x and
197 VOCs are plotted based on the simulation results.

198 3. Results and discussions

199 3.1 Overview of organic nitrates and precursors

200 The duration of the Shanghai campaign was 20 days, spanning from May 25 to June 13, 2021.
201 The analysis of organic nitrates is performed from 6 a.m. to 6 p.m., as measurements taken during
202 nighttime were subject to interference from N₂O₅ and its derivatives, a phenomenon noted in previous
203 studies (Li et al., 2021; Li et al., 2023). Simultaneous measurements of PAN and PNs were conducted
204 throughout the campaign. There was a malfunction of the GC-ECD instrument from June 12 to June
205 13, during which the measurements of PAN were generally low. Relative humidity (RH) varied
206 considerably, with over 95% during rainfall periods on June 2, June 9, June 10, and June 13, while the
207 remaining days were predominantly sunny. Temperatures were high, with minimums of 20 °C and
208 daytime peaks reaching up to 36 °C. The wind speeds were generally high during the daytime and low
209 at night, with maximum of 4.2 m/s. The easterly winds prevailed during the campaign, except for May

210 27-28 and June 3-6 with mostly west and southwest winds.



211

212 **Figure 2.** The time series of the related parameters focused on organic nitrates during the campaign. The background
213 days are represented by green B, the clean days are represented by blue C, and the ozone pollution day is represented
214 by red P.

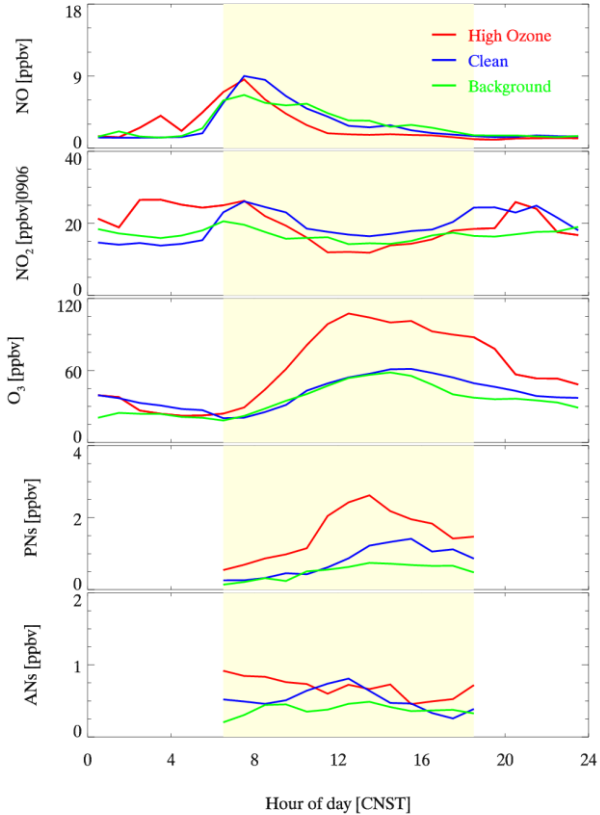
215 According to Chinese air quality standards for Class II areas, which define ozone pollution days
216 as those with an hourly average exceeding 100 ppbv, the periods from May 29 to May 30 and June 5
217 to June 6 have been identified as ozone pollution days. The days without ozone pollution are
218 categorized as clean or background days. For clean days, parameters, including KOH , SO_2 , and CO ,
219 show significant diurnal variations (Fig S1), and no rain occurs. The days that are neither ozone
220 pollution days nor clean days are then classified as background days. The daytime averages of
221 environmental parameters during the ozone pollution period, the clean period, and the background
222 period are presented in Table 2. Excluding cloudy and rainy days, the daytime peak of $J(O^1D)$ was
223 near $2.8 \times 10^5 s^{-1}$, indicating a high photochemical oxidation potential. As a secondary photochemical
224 product, O_3 exhibited a typical daily profile, peaking at 140.5 ppbv throughout the campaign. The
225 measurements of PNs peaked at 3.6 ppbv with a daytime average of 0.5 ± 0.3 ppbv, while ANs peaked
226 at 1.6 ppbv with a daytime average of 0.5 ± 0.3 ppbv. Ozone pollution periods were often associated
227 with high organic nitrates. The mean daily variation of NO_x was consistent with the characteristics of
228 typical urban sites, significantly influenced by the morning-evening rush hours. During the daytime,
229 NO exhibited a single peak distribution, whereas NO_2 displayed a bimodal distribution. In comparison
230 to the background and clean period, the ozone pollution period was characterized with higher
231 temperatures and lower humidity. Additionally, the photolysis rate and levels of $PM_{2.5}$ were both
232 elevated during pollution days.

233 **Table 2.** Summary of daytime averages of chemical parameters over different periods during the Shanghai campaign.

| Phase | Ozone pollution | Background | Clean |
|--|-----------------|-------------|-------------|
| T/°C | 29.8±3.7 | 27.0±3.4 | 26.0±3.5 |
| P/hPa | 1043.6±0.8 | 1045.3±0.9 | 1044.3±1.4 |
| RH/% | 39.2±13.9 | 65.2±16.0 | 62.4±17.2 |
| J(O ¹ D)×10 ⁵ /s | 1.3±0.9 | 0.9±0.8 | 0.8±0.8 |
| J(NO ₂)×10 ³ /s | 4.5±2.1 | 2.8±2.0 | 2.6±1.9 |
| NO ₂ /ppbv | 17.3±6.1 | 16.5±5.8 | 20.3±7.4 |
| NO/ppbv | 3.2±2.6 | 4.0±2.7 | 4.2±3.7 |
| O ₃ /ppbv | 78.6±30.9 | 41.6±27.7 | 45.0±21.5 |
| PM _{2.5} /μg·m ⁻³ | 25.9±4.3 | 18.3±13.4 | 21.9±10.0 |
| SO ₂ /ppbv | 2.2±1.7 | 0.4±0.5 | 0.6±0.7 |
| CO/ppbv | 505.3±64.3 | 441.6±133.3 | 535.0±147.8 |
| ISO/ppbv | 0.1±0.1 | 0.2±0.2 | 0.1±0.1 |

234

235 The mean diurnal profiles of organic nitrates and related parameters observed during the campaign
 236 are shown in Fig. 3. During the ozone pollution period, NO_x exhibited a peak concentration at 3:00
 237 a.m., indicating the transport of a polluted air mass to the site. In comparison to the clean period,
 238 daytime NO_x was lower during the ozone pollution period, particularly at noon when NO dropped to
 239 as low as 1.7 ppbv. Correspondingly, ANs during the ozone pollution period were generally high, but
 240 the daily variation was not significant. Therefore, the sources of ANs were more complex during the
 241 ozone pollution period, involving both transport contribution and local production, which aligns with
 242 the significantly increased background O₃. During the clean period, the daytime peak of O₃ was notably
 243 reduced and occurred later in the day. The fluctuations in NO_x were more closely associated with
 244 morning and evening rush hours. The daytime peak of PN decreased from 2.6 ppbv to 1.4 ppbv. In
 245 addition, the diurnal profile of ANs displayed a more pronounced peak at noon. During the background
 246 period, there was a further decline in the daytime peaks of NO_x compared to the clean period. The
 247 diurnal profile of O₃ exhibited similar trends, but the duration of high O₃ was significantly shortened.
 248 The levels of both PN and ANs exhibited a decline, approaching the background concentrations.



249

250 **Figure 3.** Mean diurnal profiles of organic nitrates and related parameters during different observation periods.

251 Here, we compare our observations with the study previously conducted in Xinjin, which is a
 252 suburban site, located in basin topography and faces emerging ozone pollution recently, to determine
 253 the effect of organic nitrate on O_3 production under different pollution conditions (Li et al., 2023). The
 254 Shanghai and Xinjin campaigns were conducted in early and late summer, respectively, exhibiting
 255 similar meteorological conditions. Photochemical conditions during both two campaigns are
 256 comparable, with the daily means of $J(O^1D)$ were $0.9 \times 10^{-5} \text{ s}^{-1}$ and $0.8 \times 10^{-5} \text{ s}^{-1}$, while the daily means
 257 of $J(NO_2)$ were $3.1 \times 10^{-3} \text{ s}^{-1}$ and $3.0 \times 10^{-3} \text{ s}^{-1}$, respectively, during Shanghai and Xinjin campaigns.
 258 The ratio of NO to NO_x was 0.19 and 0.17 at Shanghai and Xinjin, respectively. Meanwhile, the
 259 concentration of NO_x observed in Shanghai site (daily averages of 22.0 ppbv) is higher than that
 260 observed in Xinjin site (daily averages of 12.5 ppbv). The concentrations of SO_2 and CO at Shanghai
 261 site were 0.9 and 491.4 ppbv, while SO_2 and CO were 0.6 and 404.5 ppbv, respectively. Therefore, the
 262 air masses at Shanghai site were less aged than Xinjin site. However, the concentration of VOCs is
 263 lower in Shanghai campaign compared to Xinjin campaign, with daily mean of 23.5 ppbv compared
 264 to 22.4 ppbv. Therefore, a comparison of the two campaigns facilitates a comprehensive analysis of
 265 the impacts of organic nitrate chemistry on local ozone pollution.

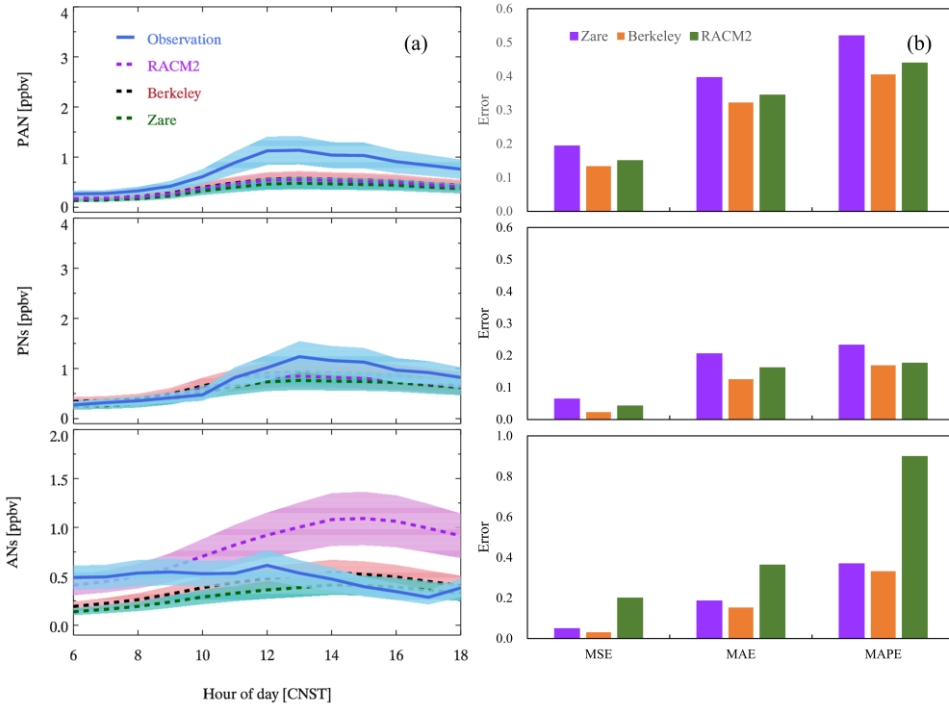
266 **3.2 Evaluation of organic nitrates simulations**

267 In light of the updates to the mechanisms, validation testing has been conducted. Our previous
 268 study of the Xinjin campaign evaluated three mechanism schemes: mechanism S0, which is based on
 269 RACM2, mechanism S1 and mechanism S2 which refines the budget for BVOC-derived organic

270 nitrates (Li et al., 2023). It was found that the performance of mechanism S2 for organic nitrates
271 exhibited an improvement exceeding 50%. Mechanism S2 has been updated by the Berkeley group
272 (Fisher et al., 2016; Travis et al., 2016), which includes enhancements to the production mechanism of
273 isoprene, the incorporation of the production mechanism for monoterpenes, and the completion of the
274 uptake of organic nitrates by aerosols. Additionally, the Zare mechanism further refines the production
275 mechanism of organic nitrates initiated by OH and NO_3 , as well as improving the deposition process
276 of organic nitrates. As a result, the Shanghai campaign was simulated using RACM2, Berkeley, and
277 Zare mechanisms respectively for comparison.

278 The simulation result of organic nitrates under the three mechanisms is shown in Fig. 4a. The
279 simulations for PAN or PNs exhibit an overall underestimation tendency, with the simulation of PAN
280 demonstrating an even greater underestimation. Notably, the measured PNs remained above 500 pptv
281 during nighttime, indicating a continuous transportation contribution at this site. Furthermore, the
282 underestimation of PNs may be attributed to the unidentified RO_x sources. It is consistent with the
283 findings from summer campaigns in Wangdu, Beijing, where an underestimation of RO_2 was noted,
284 particularly pronounced at elevated ambient NO_x (Tan et al., 2017a). In terms of ANs, the simulation
285 performances vary across different mechanisms. A significant overestimation of ANs is evident when
286 utilized RACM2. Conversely, the simulation based on the Berkeley and Zare mechanisms generally
287 results in an underestimation of ANs, while the underestimation of the Zare mechanism is more
288 significant. Sensitivity tests conducted in Xinjin campaign suggested that the simple representation of
289 ANs uptake caused the underestimation (Li et al., 2023), which is the same reason of underestimation
290 in the Shanghai campaign. The uptake of ANs need further experimental data to achieve a detailed
291 description to support the simulations.

292 The diurnal profile of simulated PNs is consistent with the measurements, both reaching their
293 daytime peak shortly after sunrise. However, it is noteworthy that the peak concentration of PNs
294 measurements is significantly higher than the simulation. In a similar pattern with PNs, the simulated
295 ANs began to accumulate around 6:00 a.m. The measured ANs reached their peak near noon, whereas
296 the simulations peaked at 3:00 pm. To evaluate the performance of simulations, as showed in Fig. 4b,
297 three types of error ratios were calculated: Mean Square Error (MSE), Mean Absolute Error (MAE),
298 and Mean Absolute Percentage Error (MAPE). Different error metrics for the organic nitrates exhibit
299 a similar trend. The simulation performances of the Berkeley mechanism are better than the other two
300 mechanisms. It should be noted that the Berkeley mechanism failed to fully reproduce the diurnal
301 pattern of observed ANs. This is mainly due to the atmospheric transport that contributes to the ANs
302 as mentioned in section 3.1. In addition, the drastic changes in NO_x during rush hours will introduce
303 errors to the ANs measurements. In addition, the Zare mechanism refined the oxidation of BVOCs by
304 OH or NO_3 by introducing extra species with uncertain yields, which might bring biases to the
305 simulations under high NO_x and anthropogenic VOCs. In general, the Berkeley mechanism performs
306 better on simulation of ANs than Zare mechanism. As a result, the subsequent analysis is based on the
307 Berkeley mechanism.

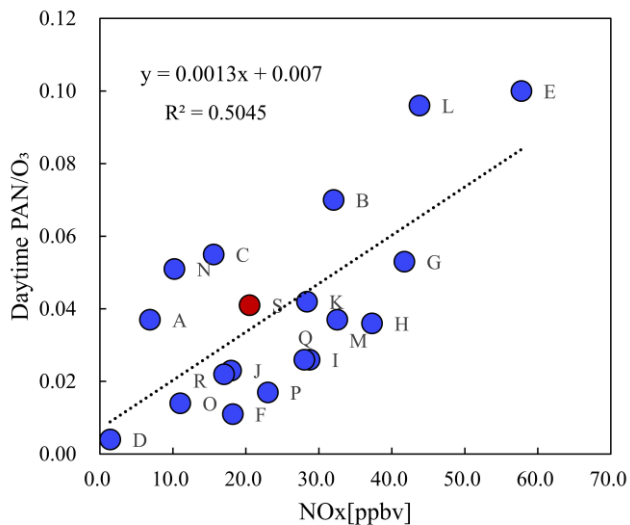


308

309 **Figure 4.** Mean diurnal profiles of observed and simulated ANs and PN_s under different mechanism constraints
 310 during the Shanghai campaign (a), and the error of the different cases (b), including mean square error (MSE), mean
 311 absolute error (MAE) and mean absolute percentage error (MAPE).

312 **3.3 Impact of PN_s chemistry on local ozone production**

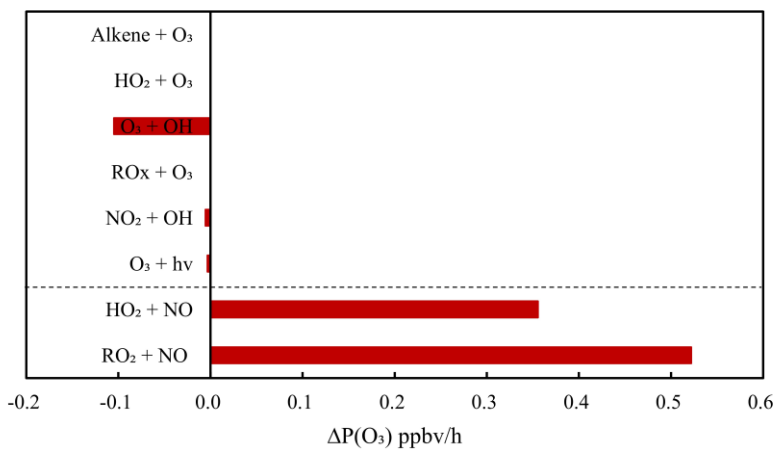
313 Organic nitrates and O₃ have common precursors, and therefore the atmospheric behavior of
 314 organic nitrates has an important influence on the local O₃ distribution. The production of PN_s
 315 consumes NO₂ and RO_x, thereby directly impacting O₃ production. The relationship between the
 316 distribution of PN_s and O₃ is examined throughout the campaign. The observed PAN, PN_s and O₃
 317 between 9:00 a.m. and 2:00 p.m. are selected for the analysis to mitigate interference from sources that
 318 are not produced during daytime. The correlation of PAN or PN_s with O₃ are shown in Fig. S2. Both
 319 PAN and PN_s demonstrate a strong correlation with O₃ with the ratio of PAN or PN_s to O₃ being 0.041
 320 or 0.058. High ratios of PN_s and O₃ usually indicate severe pollution episodes (Shepson et al., 1992;
 321 Sun et al., 2020; Zhang et al., 2023; Zhang et al., 2014). The minimum ratio of PN_s to O₃ (0.024) was
 322 found during the clean periods, which can be regarded as the threshold for local photochemical
 323 pollution. NO_x is the key pollutant for production of O₃ and PN_s, in order to study the relationship
 324 between the ratio of PAN or PN_s to O₃ and NO_x. The daytime ratios of PAN to O₃ derived from
 325 historical field observations are summarized with corresponding NO_x concentrations in Fig. 5. The
 326 ratio derived from this study was distributed in the medium level of historical observations. The linear
 327 correlation of NO_x and the ratio of PAN to O₃ ratio suggests that the NO_x concentration controls the
 328 relative production of PN_s and O₃.



329

330 **Figure 5.** The relationship between historical daytime ratio of PAN to O₃ and NO_x concentrations. The red dot is the
 331 Shanghai campaign, and the blue dots are the historical campaigns. A: Grosjean et al., 2002 (Grosjean et al., 2002);
 332 B: Lee et al., 2008 (Lee et al., 2008), C: Zhang et al., 2014 (Zhang et al., 2014), D-E: Zhang et al., 2009 (Zhang et
 333 al., 2009), F-G: Zeng et al., 2019 (Zeng et al., 2019), H-K: Zhang et al., 2019 (Zhang et al., 2019), L-M: Sun et al.,
 334 2020 (Sun et al., 2020); N: Li et al., 2023 (Li et al., 2023), O-R: Xu et al., 2024 (Xu et al., 2024), S: this study.

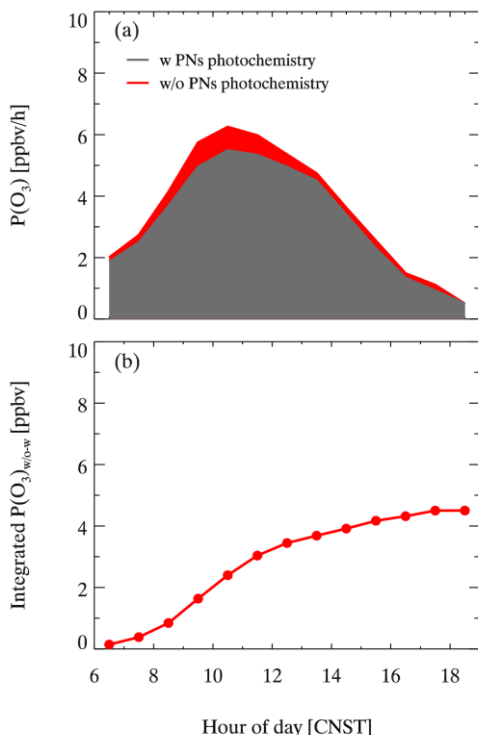
335 Sensitivity tests were conducted based on the box model to quantify the impact of PN
 336 photochemistry on O₃ budgets. The differences of each pathway rate are calculated at the peak of O₃
 337 production rate (Fig. 6). In the absence of PN photochemistry, two primary source pathways -namely, the
 338 reaction between RO₂ and NO, and the reaction between HO₂ and NO-exhibit large enhancements of
 339 0.52 and 0.36 ppbv/h, respectively. In comparison, O₃ sinks increase slightly in the absence of PN
 340 photochemistry, with the reaction between OH and O₃ showing the most significant enhancement of
 341 0.11 ppbv/h. Therefore, during the Shanghai campaign, PN photochemistry suppressed daytime ozone
 342 production mainly by reducing the reaction between HO₂ or RO₂ and NO.



343

344 **Figure 6.** The simulated difference of ozone produce rate (ΔP(O₃)) at 11am between the constraint of the PN
 345 photochemistry and without the PN photochemistry.

346 The PNs maintain a notable concentration until 6:00 p.m., suggesting a persistent impact on local
 347 ozone production. As shown in Fig. 7a, the PNs photochemistry began to inhibit ozone production as
 348 early as 6 a.m. and increased up to 0.8 ppbv/h (16%) at 10 a.m. The integrated inhibition of PNs
 349 photochemistry on O_3 production was 4.5 ppbv in the Shanghai campaign (Fig. 7b), which was less
 350 pronounced than the Xinjin campaign (20 ppbv). The reduced inhibition can be attributed to the lower
 351 PNs production rate ($P(PNs)$) observed in the Shanghai campaign (Fig. S3), where the maximum
 352 daytime $P(PNs)$ was 0.89 ppbv/h, much lower than that in Xinjin campaign (3.09 ppbv/h). In addition,
 353 the two campaigns had similar concentrations of VOCs, but daytime average of NO_x in Shanghai site
 354 is 22.0 ppbv, which is much higher than that of Xinjin site (10.2 ppbv). The PNs formation would be
 355 reduced under high NO_x condition due to the rapid termination reaction via OH and NO_2 , and thus
 356 limited the suppression effect of PNs formation which is the case in Shanghai campaign. Like in Xinjin
 357 campaign, PAN chemistry suppressed O_3 formation at a rate of 2.84 ppbv/h at a suburban site in Hong
 358 Kong (Zeng et al., 2019). However, it was reported that PAN tended to suppress O_3 production under
 359 low- NO_x and low- RO_x conditions but enhanced O_3 production with sufficient NO_x at a rural coastal
 360 site in Qingdao, which is consistent with the comparison of Xinjin and Shanghai campaigns (Liu et al.,
 361 2021). The impacts of PNs photochemistry on O_3 vary across different days. As shown in Fig. S4, the
 362 integrated $P(O_3)$ change reaches 6.9 ppbv due to PNs photochemistry during ozone pollution period.
 363 For the background and clean periods, the changes are close to each other with a value of 3.8 and 4.2
 364 ppbv, respectively. Therefore, the PNs photochemistry contributes to more $P(O_3)$ inhibition during the
 365 ozone pollution period, which should be considered in ozone pollution prevention.

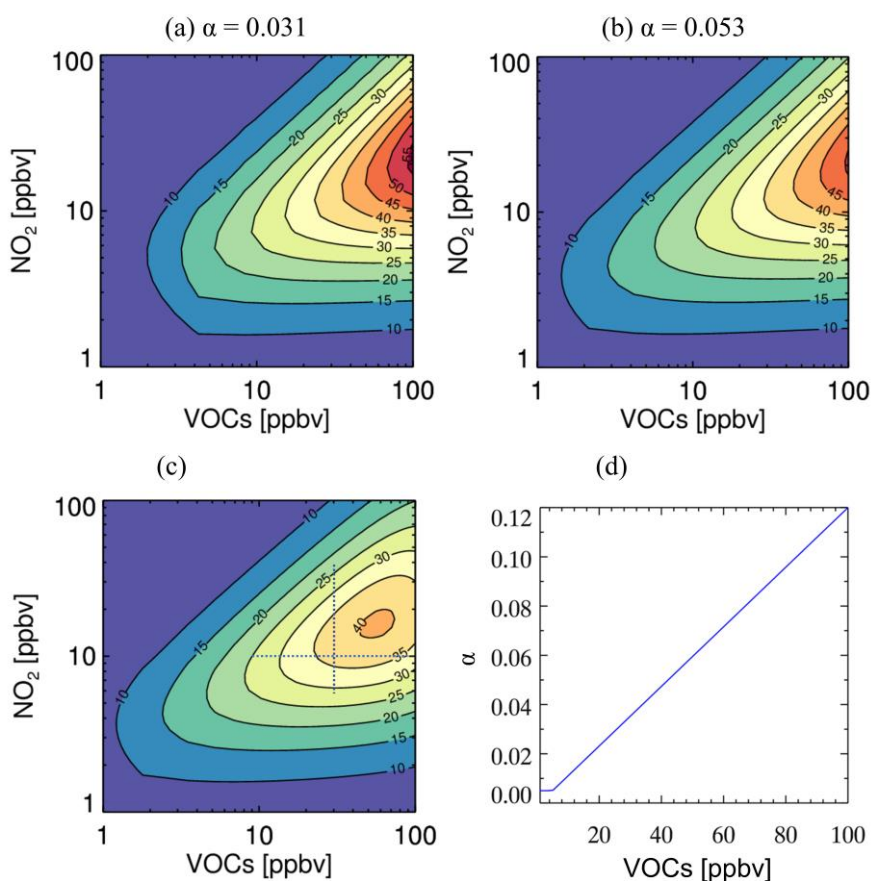


366

367 **Figure 7.** The impact of PNs photochemistry on $P(O_3)$ during the Shanghai campaign (a) daily changes of $P(O_3)$
 368 under the constraint of PNs photochemistry, (b) integrated $P(O_3)$ change constrained by PNs photochemistry.

369 **3.4 Impact of ANs chemistry on local ozone production**

370 To elucidate the impact of the α on O_3 production, the EKMA was utilized to investigate the
 371 combined response of NO_x and VOCs to O_3 production at different α . The O_3 production was calculated
 372 by a simplified approach in method 2.2 and the α values were derived from weighted average of α
 373 based on the measured VOCs, the corresponding OH reaction rate constant and the α (Table S1) in
 374 Shanghai and Xinjin campaign, respectively. The model is initiated by the daytime averages of the
 375 environmental parameters. A comparative analysis is conducted between the Xinjin campaign and the
 376 Shanghai campaign where effective α is determined to be 0.031 and 0.053, respectively. As illustrated
 377 in Fig. 8a&b, $P(O_3)$ exhibits a similar trend with the variations of NO_x and VOCs under different α ,
 378 while the value of $P(O_3)$ reduces with larger α at the same levels of precursors. For example, when
 379 VOCs is at 8 ppbv and NO_x reaches 9 ppbv, the $P(O_3)$ is 30.4 ppbv/h with α of 0.031, whereas it
 380 decreases to 24.6 ppbv/h when α is 0.053. In addition, the larger of α in the Shanghai campaign
 381 increases the threshold of NO_x concentration for the transition of O_3 production regime. When the
 382 concentration of VOCs is fixed, a higher effective α results in a lower NO_x concentration corresponding
 383 to the peak of $P(O_3)$. Consequently, an increase in α suppresses the peak of $P(O_3)$ and simultaneously
 384 affects its sensitivity to NO_x and VOCs concentrations.



385

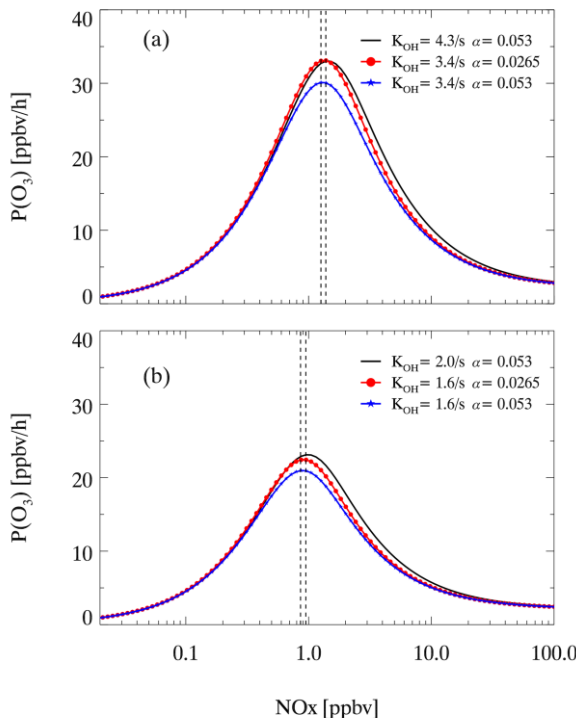
386 **Figure 8.** Ozone production ($P(O_3)$, ppb h⁻¹) derived from a simplified analytic model is plotted as a function of NO_x
 387 and VOCs under three different organic nitrate scenarios with branching ratios of (a) 0.031 for the Xinjin campaign,
 388 (b) 0.053 for the Shanghai campaign, and (c)VOC-dependent branching ratios for Shanghai campaign, where the

389 branching ratio decreases linearly from 12 to 0.5% with VOCs from 100 to 5 ppbv as shown in (d).

390 In the real atmosphere, the effective α of ANs tends to exhibit a decline with the reduction of
391 VOCs concentration. Historical studies show the general range from 0.03 to 0.04 in rural sites and
392 from 0.04 to 0.10 in urban environments, depending on the composition of VOCs and the α for BVOCs
393 (Farmer et al., 2011; Perring et al., 2010; Perring et al., 2013; Perring et al., 2009; Rosen et al., 2004b).
394 For simplicity, we use a linear relationship between α and VOC concentration in the sensitivity analysis,
395 as shown in Fig. 8d. An α value of 0.005 was selected for clean condition with VOC concentration less
396 than 5 ppbv, while 0.12 was selected for polluted condition with VOC concentration larger than 100
397 ppbv. The lower limit of 0.005 is the average of the α for methane and ethylene. The upper limit of
398 0.12 is set as the reported value of the α for isoprene and the α for aromatic hydrocarbons are generally
399 distributed around 0.1 (Perring et al., 2013). The assumption of this linear relationship between α and
400 VOC concentration has also been applied in a previous study (Farmer et al., 2011). With a varying α ,
401 as shown in Fig. 8d, $P(O_3)$ does not follow a consistent downward trend as VOCs decrease in VOC-
402 limited regime or transition regime. Instead, with the decrease of VOCs, the $P(O_3)$ is likely to increase
403 at first at a relatively high VOCs distribution, and then decrease similar to the fixed α scenario. Take
404 the cases of the horizontal dashed line as an example, at a fixed NO_x , the $P(O_3)$ increases as the VOCs
405 decrease within the range of about 60 to 100 ppbv, whereas $P(O_3)$ subsequently decrease as VOCs fell
406 below 60 ppbv. Therefore, with the reduction in VOCs emission, an increase in α directly correlates
407 with a reduction in the $P(O_3)$ peak. As a result, a positive correlation between α and VOCs
408 concentrations in real atmosphere might alter the NO_x -VOCs- O_3 relationship and diminish the effects
409 of VOCs reduction on ozone control.

410 Scenarios with different VOCs reactivity and α are selected for sensitivity tests to further
411 investigate the impact of ANs chemistry on the O_3 pollution control strategy in Shanghai. As illustrated
412 in Fig. 9a, variations of $P(O_3)$ among three scenarios exhibit an initial increase followed by a
413 subsequent decrease with rising NO_x . For the typical VOC reactivity and α obtained from the Shanghai
414 campaign, the turning point from NO_x benefit to NO_x limitation for $P(O_3)$ occurs at NO_x concentration
415 of 1.38 ppbv, when $P(O_3)$ reaches a peak of 33.0 ppbv/h. When VOCs are reduced by 20% without
416 accounting for the reductions in α , the turning point for NO_x decreases to 1.26 ppbv with the $P(O_3)$
417 peak decreasing to 30.1 ppbv/h. When the reduction of α is considered alongside the decrease in VOCs
418 (α decreases to 0.0265), the peak of $P(O_3)$ remains the same as the initial case. Consequently,
419 neglecting the α changes is likely to overestimate the effectiveness of emission control. Our
420 observations indicated that NO_x in Shanghai was notably high, which accords with the conditions to
421 the right of the turning point in Fig. 9a. In this case, the major chain-termination reaction of the HO_x
422 cycle is the reaction between OH and NO_2 to produce HNO_3 , while the share of the reaction that
423 produces ANs through the reaction between RO_2 and NO becomes relatively minor. As illustrated in
424 Fig. 9a, when NO_x changes from 22.0 to 1.0 ppbv, the impact of α change will be larger, as the $P(O_3)$
425 difference between the two cases ranges from 0.1 to 2.6 ppbv/h. Therefore, the variation of α has a
426 limited impact on O_3 production at high NO_x , whereas it offsets the impact of VOCs reduction as NO_x
427 decrease to around 1.5 ppbv which represents a low- NO_x emission condition. In addition, the
428 sensitivity analyses in a reduced VOC condition show that neglecting the α change still overestimates
429 the impact of VOCs reduction on $P(O_3)$ by around 4 times with NO_x of 1 ppbv (Fig. 9b), which is also
430 more significant than the case in Shanghai campaign. Therefore, the variation in α has a temporarily
431 limited impact on O_3 production, whereas it should be seriously considered as NO_x levels continue to

432 decrease.



433

434 **Figure 9.** The ozone production rate ($P(O_3)$) varies as a function of NO_x under different VOC- NO_x regimes
435 during Shanghai campaign: (a) under mean measured parameters during the whole campaign (solid line, VOC
436 reactivity (K_{OH}) of 4.3/s, ANs branching ratio (α) of 0.053); a 20% reduction in K_{OH} with a 50% reduction in α
437 (red dot line, 3.4/s, 0.0265); a 20% reduction in K_{OH} with no change in α (blue dot line, 3.4/s, 0.053). (b) under
438 observed parameters during the clean days (solid line, K_{OH} of 2.0/s, α of 0.053); a 20% reduction in K_{OH} with a
439 50% reduction in α (red dot line, 1.6/s, 0.0265); a 20% reduction in K_{OH} with no change in α (blue dot line, 1.6/s,
440 0.053). Dash lines show the turning point in different cases.

441 To further investigate the effect of ANs formation on O_3 production during different days,
442 sensitivity tests on VOCs reactivity and α are conducted based on typical conditions during different
443 periods. The α values are derived as 0.055, 0.054 and 0.052, for the high ozone, clean and background
444 periods, respectively. As shown in Fig. S4, the $P(O_3)$ exhibits a similar trend with the increase of NO_x
445 across different periods. The $P(O_3)$ peak during the background period (30.3 ppbv/h) is slightly lower
446 than that during both the high ozone days and the clean days (32.5 and 32.4 ppbv/h). Therefore, the
447 ANs chemistry has similar effects on O_3 production within different periods during the Shanghai
448 campaign. Further comparisons of ozone production under varying precursor levels were conducted
449 using historical observations collected in August 1994 at Mecklenburg-Vorpommern Mankmoos (MK),
450 Germany (Ehhalt, 1999), and during the spring of 2006 in Mexico City (MX) (Farmer et al., 2011;
451 Perring et al., 2010). The MK site serves as a typical clean background location with a very low
452 effective α of 0.005, corresponding to τ_{VOC} of 0.4 s⁻¹, where methane is the predominant pollutant.
453 Conversely, the MX site is characterized as an urban environment with an effective α of 0.036, where
454 a total of 58 VOCs was measured, corresponding to τ_{VOC} of 3.1 s⁻¹. The MK site shows a peak of
455 $P(O_3)$ is 2.2 ppbv/h at the NO_x of 0.63 ppbv. In contrast, the MX site demonstrates a peak $P(O_3)$ of 7.2
456 ppbv/h at a NO_x of 1.9 ppbv. Given that the Xinjin and Shanghai sites exhibit higher VOCs reactivity

457 than MX, the corresponding peak $P(O_3)$ and the NO_x inflection point are significantly elevated. This
458 increase is primarily attributed to the high $P(HO_x)$, coupled with a low α , which substantially enhances
459 $P(O_3)$ under the intensified HO_x cycling. Consequently, the ozone production potentials of urban sites
460 in China are overall higher than in other regions, while the influence of α appears to be weak.

461 **4. Conclusions**

462 This study reveals the abundances of PNs and ANs and quantifies their respective impacts on O_3
463 pollution based on the field campaign in Shanghai. They both showed higher values but less
464 pronounced diurnal variation during the O_3 pollution period than the clean period. The mechanism
465 validation indicates that Berkeley mechanism generally outperforms in the simulation of organic
466 nitrates. The ratio of PNs/ O_3 serves as a significant indicator of photochemistry. In comparison to the
467 previous Xinjin campaign, the inhibition effect of PNs chemistry on daytime O_3 production diminished,
468 likely attributed to the lower production of PNs. For ANs, the model simulation demonstrated that the
469 branching ratio (α) influences the NO_x -VOCs- O_3 sensitivity. The consideration of α value not only
470 alters the $P(O_3)$ peak in EKMA but also resulted in low effectiveness of precursor reductions, as the α
471 would change with the reduction of VOCs. It is worth mentioning that the complex polluted regions
472 are usually characterized by high NO_x and HO_x . In that case, the contribution of chain-termination
473 reactions that produce ANs could be reduced, leading to limited impact of AN chemistry on O_3
474 formation. The effect of ANs chemistry on O_3 pollution control is therefore expected to enhance with
475 further precursor reductions, and we suggest a pressing need for more measurements and analysis of
476 organic nitrates to address the forthcoming challenges in air pollution mitigation.

477
478 **Code/Data availability.** The datasets used in this study are available from the corresponding author
479 upon request (chenxr95@mail.sysu.edu.cn; k.lu@pku.edu.cn).

480
481 **Author contributions.** K.D.L. and X.R.C. designed the study. C.M.L. and X.R.C. analyzed the data
482 and wrote the paper with input from K.D.L.

483
484 **Competing interests.** The authors declare that they have no conflicts of interest.

485
486 **Acknowledgments.** This work was supported by the National Natural Science Foundation of China
487 (Grants No. 42407139); the National Natural Science Foundation of China (Grants No. 22406204);
488 the special fund of State Environmental Protection Key Laboratory of Formation and Prevention of
489 Urban Air Pollution Complex (SEPAir-2024080219); the Innovative Exploration Program of National
490 Institute of Metrology, China (No. AKYCX2313).

References

493 Arey J, Aschmann SM, Kwok ESC, Atkinson R. Alkyl Nitrate, Hydroxyalkyl Nitrate, and Hydroxycarbonyl Formation
494 from the NO_x–Air Photooxidations of C5–C8 n-Alkanes. *The Journal of Physical Chemistry A* 2001; 105: 1020–
495 1027.

496 Aruffo E, Di Carlo P, Dari-Salisburgo C, Biancofiore F, Giammaria F, Busilacchio M, et al. Aircraft observations of the
497 lower troposphere above a megacity: Alkyl nitrate and ozone chemistry. *Atmospheric Environment* 2014; 94: 479–
498 488.

499 Ashmore MR. Assessing the future global impacts of ozone on vegetation. *Plant Cell and Environment* 2005; 28: 949–964.

500 Browne EC, Cohen RC, Wooldridge PJ, Valin LC, Min K-E. Organic nitrate formation: Impacts on NO_x lifetime and ozone.
501 Abstracts of Papers of the American Chemical Society 2012; 244.

502 Browne EC, Min KE, Wooldridge PJ, Apel E, Blake DR, Brune WH, et al. Observations of total RONO₂ over the boreal
503 forest: NO_x sinks and HNO₃ sources. *Atmospheric Chemistry and Physics* 2013; 13: 4543–4562.

504 Chen J, Wu H, Liu AW, Hu SM, Zhang J. Field Measurement of NO₂ and RNO₂ by Two-Channel Thermal Dissociation
505 Cavity Ring Down Spectrometer. *Chinese Journal of Chemical Physics* 2017; 30: 493–498.

506 Darer AI, Cole-Filipliak NC, O'Connor AE, Elrod MJ. Formation and Stability of Atmospherically Relevant Isoprene-
507 Derived Organosulfates and Organonitrates. *Environmental Science & Technology* 2011; 45: 1895–1902.

508 Day DA, Dillon MB, Wooldridge PJ, Thornton JA, Rosen RS, Wood EC, et al. On alkyl nitrates, O-3, and the "missing
509 NO_y". *Journal of Geophysical Research-Atmospheres* 2003; 108.

510 Ehhalt DH. Photooxidation of trace gases in the troposphere. *Physical Chemistry Chemical Physics* 1999; 1: 5401–5408.

511 Farmer DK, Perring AE, Wooldridge PJ, Blake DR, Baker A, Meinardi S, et al. Impact of organic nitrates on urban ozone
512 production. *Atmospheric Chemistry and Physics* 2011; 11: 4085–4094.

513 Fisher JA, Jacob DJ, Travis KR, Kim PS, Marais EA, Miller CC, et al. Organic nitrate chemistry and its implications for
514 nitrogen budgets in an isoprene- and monoterpene-rich atmosphere: constraints from aircraft (SEAC(4)RS) and
515 ground-based (SOAS) observations in the Southeast US. *Atmospheric Chemistry and Physics* 2016; 16: 5969–5991.

516 Flocke F, Volz-Thomas A, Buers HJ, Patz W, Garthe HJ, Kley D. Long-term measurements of alkyl nitrates in southern
517 Germany 1. General behavior and seasonal and diurnal variation. *Journal of Geophysical Research-Atmospheres* 1998;
518 103: 5729–5746.

519 Gao W, Tie X, Xu J, Huang R, Mao X, Zhou G, et al. Long-term trend of O-3 in a mega City (Shanghai), China:
520 Characteristics, causes, and interactions with precursors. *Science of the Total Environment* 2017; 603: 425–433.

521 Grosjean E, Grosjean D, Woodhouse LF, Yang YJ. Peroxyacetyl nitrate and peroxypropionyl nitrate in Porto Alegre, Brazil.
522 Atmospheric Environment 2002; 36: 2405–2419.

523 Ito A, Sillman S, Penner JE. Global chemical transport model study of ozone response to changes in chemical kinetics and
524 biogenic volatile organic compounds emissions due to increasing temperatures: Sensitivities to isoprene nitrate
525 chemistry and grid resolution. *Journal of Geophysical Research-Atmospheres* 2009; 114.

526 Lee G, Jang Y, Lee H, Han J-S, Kim K-R, Lee M. Characteristic behavior of peroxyacetyl nitrate (PAN) in Seoul megacity,
527 Korea. *Chemosphere* 2008; 73: 619–628.

528 Li C, Wang H, Chen X, Zhai T, Chen S, Li X, et al. Thermal dissociation cavity-enhanced absorption spectrometer for
529 measuring NO₂, RO₂NO₂, and RONO₂ in the atmosphere. *Atmospheric Measurement Techniques* 2021; 14: 4033–
530 4051.

531 Li C, Wang H, Chen X, Zhai T, Ma X, Yang X, et al. Observation and modeling of organic nitrates on a suburban site in
532 southwest China. *Science of the Total Environment* 2023; 859.

533 Liebmann J, Karu E, Sobanski N, Schuladen J, Ehn M, Schallhart S, et al. Direct measurement of NO₃ radical reactivity
534 in a boreal forest. *Atmospheric Chemistry and Physics* 2018; 18: 3799–3815.

535 Liebmann J, Sobanski N, Schuladen J, Karu E, Hellen H, Hakola H, et al. Alkyl nitrates in the boreal forest: formation via
536 the NO₃-, OH- and O-3-induced oxidation of biogenic volatile organic compounds and ambient lifetimes.
537 *Atmospheric Chemistry and Physics* 2019; 19: 10391–10403.

538 Ling ZH, Guo H, Simpson IJ, Saunders SM, Lam SHM, Lyu XP, et al. New insight into the spatiotemporal variability and
539 source apportionments of C-1-C-4 alkyl nitrates in Hong Kong. *Atmospheric Chemistry and Physics* 2016; 16: 8141–
540 8156.

541 Liu Y, Shen H, Mu J, Li H, Chen T, Yang J, et al. Formation of peroxyacetyl nitrate (PAN) and its impact on ozone
542 production in the coastal atmosphere of Qingdao, North China. *Science of the Total Environment* 2021; 778.

543 Lu KD, Hofzumahaus A, Holland F, Bohn B, Brauers T, Fuchs H, et al. Missing OH source in a suburban environment near
544 Beijing: observed and modelled OH and HO₂ concentrations in summer 2006. *Atmospheric
545 Chemistry and Physics* 2013; 13: 1057–1080.

546 Monks PS, Archibald AT, Colette A, Cooper O, Coyle M, Derwent R, et al. Tropospheric ozone and its precursors from the
547 urban to the global scale from air quality to short-lived climate forcer. *Atmos. Chem. Phys.* 2015; 15: 8889–8973.

548 Ng NL, Brown SS, Archibald AT, Atlas E, Cohen RC, Crowley JN, et al. Nitrate radicals and biogenic volatile organic

549 compounds: oxidation, mechanisms, and organic aerosol. *Atmospheric Chemistry and Physics* 2017; 17: 2103-2162.
550 Perring AE, Bertram TH, Farmer DK, Wooldridge PJ, Dibb J, Blake NJ, et al. The production and persistence of Sigma
551 RONO₂ in the Mexico City plume. *Atmospheric Chemistry and Physics* 2010; 10: 7215-7229.
552 Perring AE, Pusede SE, Cohen RC. An Observational Perspective on the Atmospheric Impacts of Alkyl and Multifunctional
553 Nitrates on Ozone and Secondary Organic Aerosol. *Chemical Reviews* 2013; 113: 5848-5870.
554 Perring AE, Wisthaler A, Graus M, Wooldridge PJ, Lockwood AL, Mielke LH, et al. A product study of the isoprene+NO₃
555 reaction. *Atmospheric Chemistry and Physics* 2009; 9: 4945-4956.
556 Present PSR, Zare A, Cohen RC. The changing role of organic nitrates in the removal and transport of NO_x. *Atmospheric
557 Chemistry and Physics* 2020; 20: 267-279.
558 Reisen F, Aschmann SM, Atkinson R, Arey J. 1,4-hydroxycarbonyl products of the OH radical initiated reactions of C-5-
559 C-8 n-alkanes in the presence of NO. *Environmental Science & Technology* 2005; 39: 4447-4453.
560 Roberts JM, Bertman SB. The thermal-decomposition of peroxyacetic nitric anhydride (pan) and peroxymethacrylic nitric
561 anhydride (MPAN). *International Journal of Chemical Kinetics* 1992; 24: 297-307.
562 Romer PS, Duffey KC, Wooldridge PJ, Allen HM, Ayres BR, Brown SS, et al. The lifetime of nitrogen oxides in an
563 isoprene-dominated forest. *Atmospheric Chemistry and Physics* 2016; 16: 7623-7637.
564 Romer PS, Duffey KC, Wooldridge PJ, Edgerton E, Baumann K, Feiner PA, et al. Effects of temperature-dependent NO_x
565 emissions on continental ozone production. *Atmospheric Chemistry and Physics* 2018; 18: 2601-2614.
566 Rosen RS, Wood EC, Wooldridge PJ, Thornton JA, Day DA, Kuster W, et al. Observations of total alkyl nitrates during
567 Texas Air Quality Study 2000: Implications for O₃ and alkyl nitrate photochemistry. *Journal of Geophysical
568 Research-Atmospheres* 2004a; 109: 15.
569 Rosen RS, Wood EC, Wooldridge PJ, Thornton JA, Day DA, Kuster W, et al. Observations of total alkyl nitrates during
570 Texas Air Quality Study 2000: Implications for O₃ and alkyl nitrate photochemistry. *Journal of Geophysical
571 Research-Atmospheres* 2004b; 109.
572 Sadanaga Y, Takaji R, Ishiyama A, Nakajima K, Matsuki A, Bandow H. Thermal dissociation cavity attenuated phase shift
573 spectroscopy for continuous measurement of total peroxy and organic nitrates in the clean atmosphere. *Review of
574 Scientific Instruments* 2016; 87.
575 Schwantes RH, Emmons LK, Orlando JJ, Barth MC, Tyndall GS, Hall SR, et al. Comprehensive isoprene and terpene gas-
576 phase chemistry improves simulated surface ozone in the southeastern US. *Atmospheric Chemistry and Physics* 2020;
577 20: 3739-3776.
578 Shepson PB, Hastie DR, So KW, Schiff HI. Relationships between PAN, PPN and O₃ at urban and rural sites in Ontario.
579 *Atmospheric Environment Part a-General Topics* 1992; 26: 1259-1270.
580 Song J, Zhang Y, Huang Y, Ho KF, Yuan Z, Ling Z, et al. Seasonal variations of C-1-C-4 alkyl nitrates at a coastal site in
581 Hong Kong: Influence of photochemical formation and oceanic emissions. *Chemosphere* 2018; 194: 275-284.
582 Sun J, Li Z, Xue L, Wang T, Wang X, Gao J, et al. Summertime C-1-C-5 alkyl nitrates over Beijing, northern China: Spatial
583 distribution, regional transport, and formation mechanisms. *Atmospheric Research* 2018; 204: 102-109.
584 Sun M, Cui Jn, Zhao X, Zhang J. Impacts of precursors on peroxyacetyl nitrate (PAN) and relative formation of PAN to
585 ozone in a southwestern megacity of China. *Atmospheric Environment* 2020; 231.
586 Tan Z, Fuchs H, Lu K, Hofzumahaus A, Bohn B, Broch S, et al. Radical chemistry at a rural site (Wangdu) in the North
587 China Plain: observation and model calculations of OH, HO₂ and RO₂ radicals. *Atmos. Chem. Phys.* 2017a; 17: 663-
588 690.
589 Tan Z, Fuchs H, Lu K, Hofzumahaus A, Bohn B, Broch S, et al. Radical chemistry at a rural site (Wangdu) in the North
590 China Plain: observation and model calculations of OH, HO₂ and RO₂ radicals. *Atmospheric Chemistry and Physics* 2017b; 17: 663-690.
591 Tan Z, Lu K, Jiang M, Su R, Dong H, Zeng L, et al. Exploring ozone pollution in Chengdu, southwestern China: A case
592 study from radical chemistry to O₃-VOC-NO_x sensitivity. *Sci Total Environ* 2018a; 636: 775-786.
593 Tan ZF, Rohrer F, Lu KD, Ma XF, Bohn B, Broch S, et al. Wintertime photochemistry in Beijing: observations of RO_x
594 radical concentrations in the North China Plain during the BEST-ONE campaign. *Atmospheric Chemistry and Physics*
595 2018b; 18: 12391-12411.
596 Teng AP, Crounse JD, Lee L, St Clair JM, Cohen RC, Wennberg PO. Hydroxy nitrate production in the OH-initiated
597 oxidation of alkenes. *Atmospheric Chemistry and Physics* 2015; 15: 4297-4316.
598 Travis KR, Jacob DJ, Fisher JA, Kim PS, Marais EA, Zhu L, et al. Why do models overestimate surface ozone in the
599 Southeast United States? *Atmospheric Chemistry and Physics* 2016; 16: 13561-13577.
600 Wang M, Shao M, Chen W, Lu S, Wang C, Huang D, et al. Measurements of C1-C4 alkyl nitrates and their relationships
601 with carbonyl compounds and O₃ in Chinese cities. *Atmospheric Environment* 2013; 81: 389-398.
602 Wang W, Parrish DD, Wang S, Bao F, Ni R, Li X, et al. Long-term trend of ozone pollution in China during 2014-2020:
603 distinct seasonal and spatial characteristics and ozone sensitivity. *Atmospheric Chemistry and Physics* 2022; 22: 8935-
604 8949.
605

606 Xu T, Nie W, Xu Z, Yan C, Liu Y, Zha Q, et al. Investigation on the budget of peroxyacetyl nitrate (PAN) in the Yangtze
607 River Delta: Unravelling local photochemistry and regional impact. *Science of the Total Environment* 2024; 917.

608 Xue K, Zhang X. The rationale behind updates to ambient ozone guidelines and standards. *Frontiers in Public Health* 2023;
609 11.

610 Yeh GK, Ziemann PJ. Alkyl Nitrate Formation from the Reactions of C₈-C₁₄-*n*-Alkanes
611 with OH Radicals in the Presence of NO_x: Measured Yields with Essential Corrections for Gas-
612 Wall Partitioning. *Journal of Physical Chemistry A* 2014a; 118: 8147-8157.

613 Yeh GK, Ziemann PJ. Identification and Yields of 1,4-Hydroxynitrates Formed from the Reactions of C₈-C₁₆-*n*-Alkanes with OH Radicals in the Presence of NO_x. *Journal of Physical Chemistry A* 2014b; 118: 8797-8806.

616 Young PJ, Naik V, Fiore AM, Gaudel A, Guo J, Lin MY, et al. Tropospheric Ozone Assessment Report: Assessment of
617 global-scale model performance for global and regional ozone distributions, variability, and trends. *Elementa-Science
618 of the Anthropocene* 2018; 6.

619 Zare A, Romer PS, Tran N, Keutsch FN, Skog K, Cohen RC. A comprehensive organic nitrate chemistry: insights into the
620 lifetime of atmospheric organic nitrates. *Atmospheric Chemistry and Physics* 2018; 18: 15419-15436.

621 Zeng L, Fan G-J, Lyu X, Guo H, Wang J-L, Yao D. Atmospheric fate of peroxyacetyl nitrate in suburban Hong Kong and
622 its impact on local ozone pollution. *Environmental Pollution* 2019; 252: 1910-1919.

623 Zhang B, Zhao X, Zhang J. Characteristics of peroxyacetyl nitrate pollution during a 2015 winter haze episode in Beijing.
624 *Environmental Pollution* 2019; 244: 379-387.

625 Zhang G, Xia L, Zang K, Xu W, Zhang F, Liang L, et al. The abundance and inter-relationship of atmospheric peroxyacetyl
626 nitrate (PAN), peroxypropionyl nitrate (PPN), O₃, and NO_y during the wintertime in Beijing, China. *Science of the
627 Total Environment* 2020; 718.

628 Zhang H, Tong S, Zhang W, Xu Y, Zhai M, Guo Y, et al. A comprehensive observation on the pollution characteristics of
629 peroxyacetyl nitrate (PAN) in Beijing, China. *Science of the Total Environment* 2023; 905.

630 Zhang H, Xu X, Lin W, Wang Y. Wintertime peroxyacetyl nitrate (PAN) in the megacity Beijing: Role of photochemical
631 and meteorological processes. *Journal of Environmental Sciences* 2014; 26: 83-96.

632 Zhang JM, Wang T, Ding AJ, Zhou XH, Xue LK, Poon CN, et al. Continuous measurement of peroxyacetyl nitrate (PAN)
633 in suburban and remote areas of western China. *Atmospheric Environment* 2009; 43: 228-237.

634 Zhu W, Zhou M, Cheng Z, Yan N, Huang C, Qiao L, et al. Seasonal variation of aerosol compositions in Shanghai, China:
635 Insights from particle aerosol mass spectrometer observations. *Science of The Total Environment* 2021; 771: 144948.

636